JOC The Journal of Organic Chemistry

pubs.acs.org/joc Article

Mechanism of Pd/Senphos-Catalyzed *trans*-Hydroboration of 1,3-Enynes: Experimental and Computational Evidence in Support of the Unusual Outer-Sphere Oxidative Addition Pathway

Yuanzhe Zhang, Ziyong Wang, Walid Lamine, Senmiao Xu, Bo Li, Anna Chrostowska, Karinne Miqueu,* and Shih-Yuan Liu*

Cite This: *J. Org. Chem.* 2023, 88, 2415−2424 Read Online

ACCESS | Metrics & More | Article Recommendations | Supporting Information

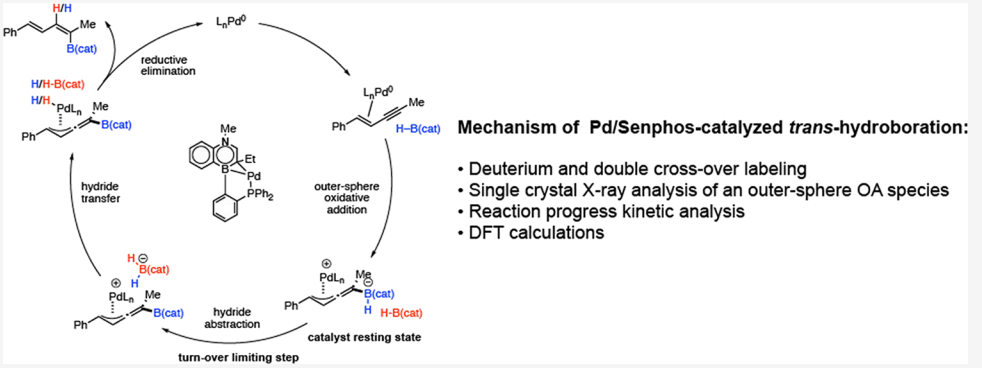

ABSTRACT: The reaction mechanism of the Pd/Senphos-catalyzed *trans*-hydroboration reaction of 1,3-enynes was investigated using various experimental techniques, including deuterium and double crossover labeling experiments, X-ray crystallographic characterization of model reaction intermediates, and reaction progress kinetic analysis. Our experimental data are in support of an unusual outer-sphere oxidative addition mechanism where the catecholborane serves as a suitable electrophile to activate the Pd^0-bound 1,3-enyne substrate to form a Pd-η^3-π-allyl species, which has been determined to be the likely resting state of the catalytic cycle. Double crossover labeling of the catecholborane points toward a second role played by the borane as a hydride delivery shuttle. Density functional theory calculations reveal that the rate-limiting transition state of the reaction is the hydride abstraction by the catecholborane shuttle, which is consistent with the experimentally determined rate law: rate = k[enyne]^0[borane]^1[catalyst]^1. The computed activation free energy $\Delta G^{\ddagger}$ = 17.7 kcal/mol and KIE (k_H/k_D = 1.3) are also in line with experimental observations. Overall, this work experimentally establishes Lewis acids such as catecholborane as viable electrophilic activators to engage in an outer-sphere oxidative addition reaction and points toward this underutilized mechanism as a general approach to activate unsaturated substrates.

INTRODUCTION

Pd-catalyzed allylic substitution has established itself as a powerful synthetic transformation for carbon−carbon and carbon−heteroatom bond formation.[1] The key organometallic intermediate is the η^3-Pd-π-allyl complex, and well-established approaches to catalytically access this species include (1) oxidative addition of allylic-type substrates in the presence of a preinstalled leaving group[2] or a stoichiometric oxidant with Pd(0) complexes,[3] (2) migratory insertion into allenes with Pd(II) complexes,[4] and (3) migratory[5] or Wacker-type[6] insertion into dienes and 1,3-enynes with Pd(II) complexes (Scheme 1).

An underexplored strategy to catalytically access the versatile η^3-Pd-π-allyl intermediate involves the activation of 1,3-dienes and 1,3-enynes by Pd(0) complexes in the presence of electrophilic activators *via* an "outer-sphere" oxidative addition mechanism (Scheme 2). In an early work, Yamamoto reported the first catalytic[7] electrophilic addition to C−C multiple bonds by a low-valent transition metal in a Pd-catalyzed hydroalkoxylation reaction of diynes.[8] More recently, Tsukamoto *et al.* described a Pd-catalyzed hydroalkylation of 1,3-enynes to furnish allenes *via* a proposed outer-sphere oxidative addition mechanism.[9] In these reports, alternative mechanisms that involve the more classical "inner-sphere" oxidative

Received: November 27, 2022
Published: February 8, 2023

https://doi.org/10.1021/acs.joc.2c02841
J. Org. Chem. 2023, 88, 2415−2424

Scheme 1. Established Catalytic Approaches to η^3-Pd-π-Allyl Complexes

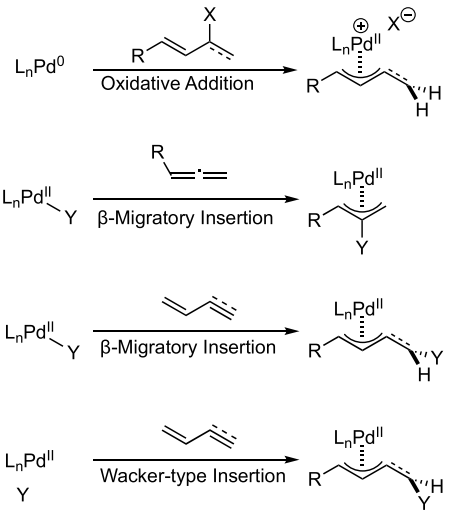

Scheme 2. Catalytically Accessing η^3-Pd-π-Allyl Complexes *via* an Uncommon Outer-Sphere Oxidative Addition Mechanism

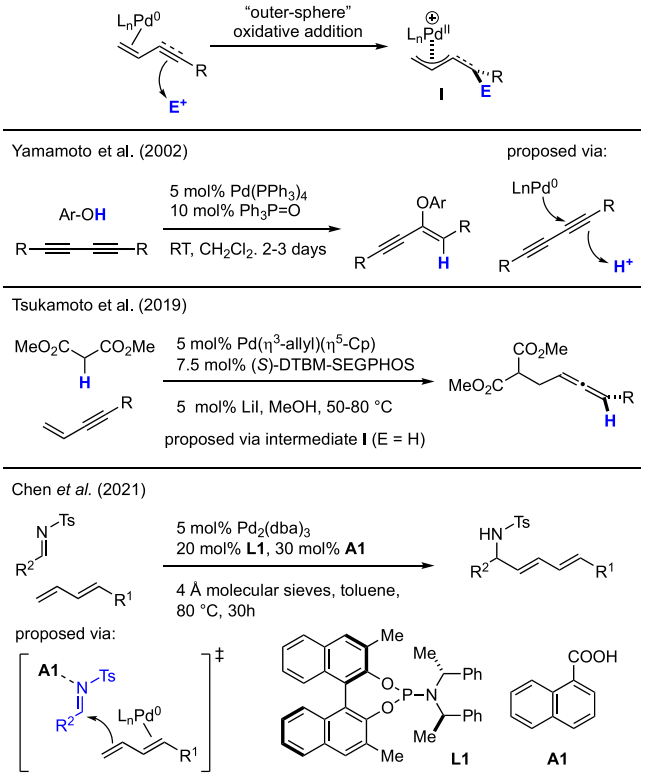

addition followed by the β-migratory insertion step have not been completely ruled out by the authors. In 2021, Chen *et al.* reported the coupling between 1,3-dienes with *N*-tosylimines as the electrophilic activator *via* an outer-sphere oxidative addition mechanism that is supported by DFT calculation.[10a] Interestingly, the corresponding coupling with 1,3-enynes as substrates (instead of 1,3-dienes) has been demonstrated to proceed *via* a "π-Lewis base catalysis" that involves an important *N*-chelation to the Pd during the oxidative addition step.[10b]

In 2016, we described the first Pd-catalyzed *trans*-selective hydroboration reaction of 1,3-enynes (Scheme 3).[11] Essential to the observed catalytic efficiency and diastereoselectivity is the use of Senphos (i.e., a 1,4-azaborine-based biaryl phosphine) as the supporting ligand.[12] Based on previously published literature on the transition-metal catalyzed *trans*-selective hydroboration reaction of alkynes,[13,14] the following mechanistic scenarios can be proposed (see Scheme 3): (1) generation of the metal vinylidene intermediate as proposed by Miyaura *et al.*[15] and Leitner *et al.*[16] for their Ir-, Rh-, and Ru-based catalysts, (2) generation of a metal acetylide intermediate as proposed by Chirik *et al.* for their Co-pincer system,[17] and (3) generation of a metallacyclopropene intermediate as proposed by Sundararaju and Fürstner for their Ru catalyst system.[18] Additional scenarios include (4) inner-sphere oxidative addition (OA) of the borane to the metal followed by *syn* β-migratory insertion (β-MI) and *cis*/*trans* isomerization and reductive elimination[19] and (5) outer-sphere oxidative addition with the borane serving as the electrophile. In 2018, Shi *et al.* reported a computational mechanistic study of the Pd/Senphos-catalyzed *trans*-hydroboration of 1,3-enynes.[20] Key features of the DFT-predicted mechanism (Scheme 3, scenario (5)) include (1) an outer-sphere oxidative addition step where an H-B(cat) cooperatively activates the Pd-bound substrate as a Lewis acid electrophile and (2) the H-B(cat) additionally serves as a hydride shuttle to deliver a hydride to the Pd catalyst in an intermolecular fashion prior to reductive elimination.

To date, no experimental mechanistic data have been reported to distinguish among the above outlined mechanistic scenarios for the Pd/Senphos-catalyzed *trans*-hydroboration of 1,3-enynes. The possibility of the outer-sphere oxidation is intriguing as our Pd-catalyzed *trans*-hydroboration would represent the first example using boron as the activating electrophile and would point toward the outer-sphere oxidative addition as a general approach for activating unsaturated compounds *via* the versatile η^3-Pd-π-allyl intermediate with possible catalyst control over site-, regio-, and diastereoselectivity. In this work, we disclose experimental mechanistic data in the form of (1) kinetic data (i.e., determination of the reaction orders and kinetic isotope effect (KIE)), (2) X-ray crystallographic data for the critical outer-sphere oxidative addition intermediate, and (3) double-crossover labeling experiment, in support of the proposed outer-sphere oxidative addition mechanism. Furthermore, we provide more refined computational results that correct a few inconsistencies between Shi *et al.*'s 2018 calculations and the experimental mechanistic observations.

RESULTS AND DISCUSSION

In our initial work, we determined that a deuterium-labeled substrate **1-D** under our reported optimized conditions gave the product without isomerization of the label (Scheme 4). This observation is inconsistent with the mechanisms involving metal vinylidene and metal acetylide intermediates (Scheme 3, scenarios (1) and (2)). Additionally, the (E)-alkene configuration of **1-D** is retained in the hydroboration product, which is inconsistent with an η^3-η^1 π-allyl walk mechanism to achieve *trans*-hydroboration selectivity after a hypothetical *syn* inner-sphere β-migratory insertion of a Pd-boryl species into the alkyne.

A key distinguishing feature of the outer-sphere oxidative addition mechanism is the proposed hydride shuttle

https://doi.org/10.1021/acs.joc.2c02841
J. Org. Chem. 2023, 88, 2415−2424

Scheme 3. Pd-Catalyzed *trans*-Hydroboration of 1,3-Enynes: Possible Mechanistic Scenarios

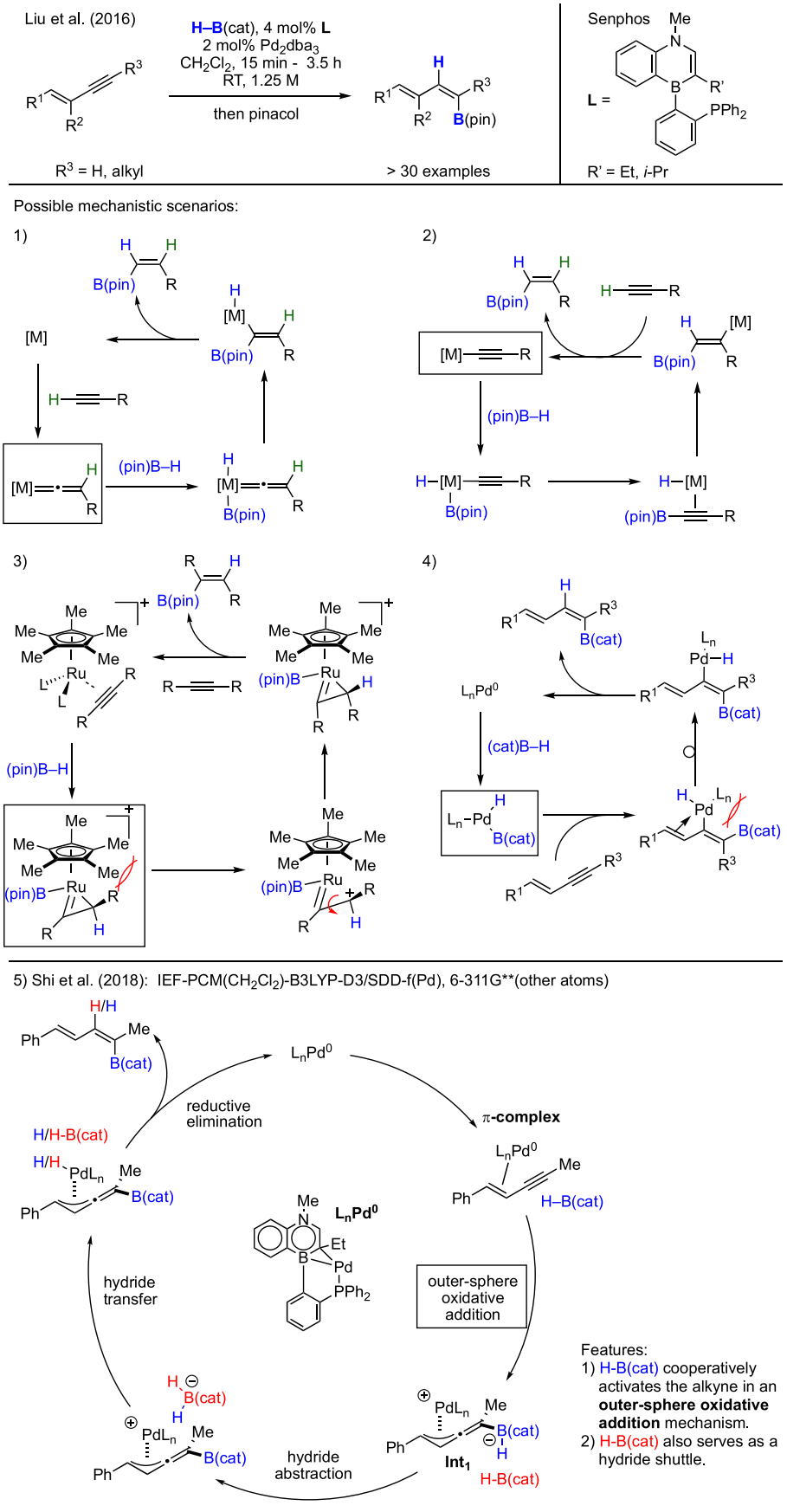

https://doi.org/10.1021/acs.joc.2c02841
J. Org. Chem. 2023, 88, 2415−2424

Scheme 4. Initial Deuterium Labeling Experiment

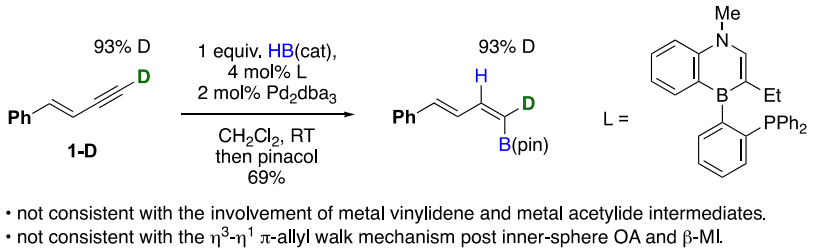

- not consistent with the involvement of metal vinylidene and metal acetylide intermediates.
- not consistent with the η^3-η^1 π-allyl walk mechanism post inner-sphere OA and β-MI.

Scheme 5. Double-Crossover Labeling Experiment is Consistent with the Hydride Shuttle Mechanism Proposed in the Outer-Sphere Oxidative Addition Scenario

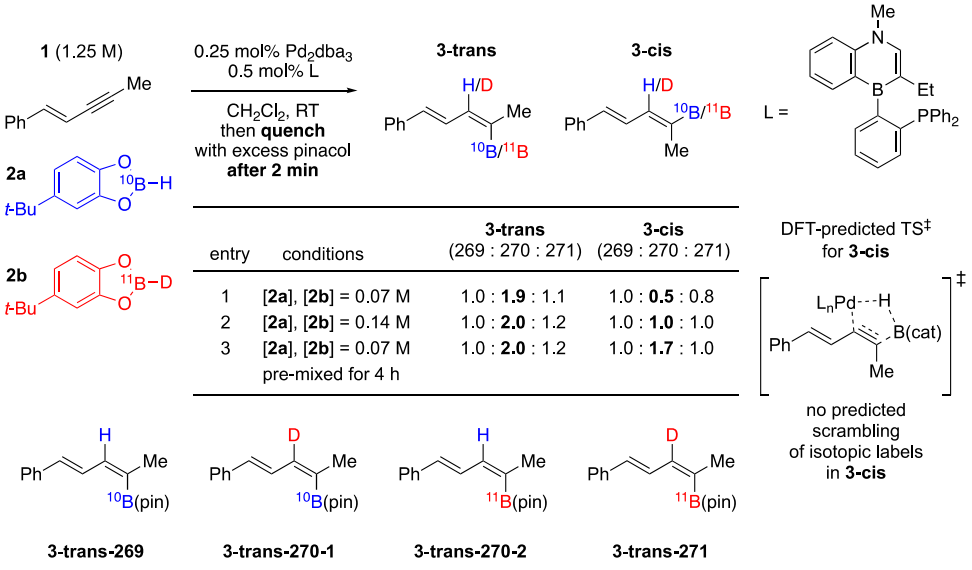

entry	conditions	3-trans (269 : 270 : 271)	3-cis (269 : 270 : 271)
1	[**2a**], [**2b**] = 0.07 M	1.0 : **1.9** : 1.1	1.0 : **0.5** : 0.8
2	[**2a**], [**2b**] = 0.14 M	1.0 : **2.0** : 1.2	1.0 : **1.0** : 1.0
3	[**2a**], [**2b**] = 0.07 M pre-mixed for 4 h	1.0 : **2.0** : 1.2	1.0 : **1.7** : 1.0

no predicted scrambling of isotopic labels in **3-cis**

3-trans-269 **3-trans-270-1** **3-trans-270-2** **3-trans-271**

mechanism where a second H-B(cat) molecule (red color in Scheme 3, scenario (5)) first abstracts a hydride from the B(cat) group (blue color) in the outer-sphere oxidative addition intermediate and then transfers it to the Pd metal prior to reductive elimination. This intermolecular hydride transfer mechanistically allows for scrambling of labels of doubly labeled (H vs D and ^{10}B vs ^{11}B) H-B(cat). To this end, we prepared the isotopically labeled[21] light ^{1}H-^{10}B(cat) (**2a**) and heavy D-^{11}B(cat) (**2b**) derivatives.[22] A double-crossover experiment was performed where the reaction was quenched at very early stages to evaluate the extent of the scrambling of the labels in the products **3-trans** and **3-cis** (Scheme 5). GC−MS was applied to detect the ratio of different isotopically labeled products based on their molecular weight. For **3-trans**, the isotopologues are **3-trans-269**, **3-trans-270-1**, **3-trans-270-2**, and **3-trans-271**, of which **3-trans-270-1** and **3-trans-270-2** are indistinguishable by MS. The corresponding isotopologues exist for the **3-cis** product, which can be detected independently by GC−MS.[23] Assuming no background scrambling, mechanistic scenarios that do not provide a mechanism for scrambling of labels such as scenario (3) (in Scheme 3), the inner-sphere oxidative addition (scenario (4) in Scheme 3), or the DFT-predicted lowest-energy transition state for the formation of **3-cis** (see Scheme 5)[20] would be predicted to produce products with Mw 269 and 271 only and none of the scrambled products with Mw 270. On the other hand, the outer-sphere oxidative mechanism (scenario (5) in Scheme 3) with the proposed hydride shuttle is predicted to give **3-trans-269**, **3-trans-270**, and **3-trans-271** in a 1.0:2.0:1.0 ratio.

Catecholboranes are known to undergo background scrambling of the B−H atoms.[24] Thus, the analysis of the isotopic ratios of the product of interest, **3-trans**, needs to be calibrated against a control compound *in situ* (i.e., **3-cis**) that informs about the extent of background scrambling. We determined that **3-cis** forms in substantial amount when the concentration of catecholborane is low relative to the optimized ([catecholborane] > 1.25 M) conditions.[25] We performed the double crossover experiments under low-borane concentrations to minimize borane background scrambling. As can be seen from Scheme 5, entry 1 ([borane] = 0.07 M), the isotopic distribution (Mw 269, 270, and 271) for **3-trans** is 1.0:**1.9**:1.1 while the corresponding isotopic distribution for the control **3-cis** is 1.0:**0.5**:0.8. This observation indicates that background borane scrambling occurs to a relatively small extent under the reaction conditions and that the observed complete scrambling of the labels in **3-trans** is induced by the reaction mechanism. Furthermore, when the borane concentration is doubled (Scheme 5, entry 2 vs entry 1), the background scrambling is accelerated as indicated by the isotopic distribution for **3-cis** (1.0:**1.0**:1.0) while the corresponding distribution for **3-trans** (1.0:**2.0**:1.2) remains essentially independent of the borane concentration. Finally, we conducted a positive control experiment where the isotopically labeled boranes **2a** and **2b** are pre-mixed for 4 h to allow for scrambling prior to being subjected to the reaction mixture. As expected, the observed isotopic ratios for both **3-**

https://doi.org/10.1021/acs.joc.2c02841
J. Org. Chem. 2023, 88, 2415−2424

trans (1.0:2.0:1.2) and **3-cis** (1.0:1.7:1.0) show substantial scrambling of the labels as a result of the background exchange. Overall, we conclude that the observed isotopic ratios of products **3-trans** and **3-cis** under the conditions shown in Scheme 5 are more consistent with the outer-sphere oxidative addition mechanism for the formation of **3-trans** (scenario (5) in Scheme 3) and not consistent with any of the other proposed scenarios illustrated in Scheme 3.

Another distinguishing feature for the outer-sphere oxidative addition mechanism is the formation of the outer-sphere oxidative addition adduct $\mathbf{Int_1}$ (see Scheme 3, scenario (5)). In our effort to provide credence to the intermediacy of the outer-sphere oxidative addition intermediate $\mathbf{Int_1}$, we employed $B(C_6F_5)_3$ as the Lewis acid activator[26] instead of the catecholborane. The hypothesis is that in the absence of a reactive hydride, the intermediate would be less reactive and therefore isolable. We are pleased to determine that the treatment of 1 equiv of LPd^0 with 4 equiv of 1,3-enyne and 1 equiv of $B(C_6F_5)_3$ produced the model outer-sphere oxidative addition intermediate $\mathbf{Int_1(BCF)}$ in 31% isolated yield (eq 1).

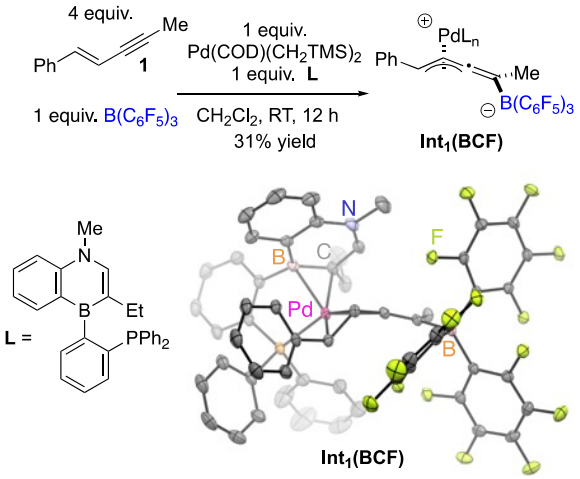

(1)

Single crystals of $\mathbf{Int_1(BCF)}$ suitable for X-ray diffraction analysis were obtained from a pentane/CH_2Cl_2 mixture at −35 °C (thermal ellipsoids in eq 2 are drawn at the 50% probability level). The structure of $\mathbf{Int_1(BCF)}$ unambiguously reveals (1) the formation of a Pd-π-allyl complex and (2) the geometrical *anti* relationship between the electrophile $B(C_6F_5)_3$ and the Pd, which are consistent with the proposed outer-sphere oxidative addition mechanism. Furthermore, the structure shows that the Senphos ligand is bound to the Pd^{II} in a κ^2-η^2-BC-coordination mode. Overall, the successful isolation and crystallographic characterization of $\mathbf{Int_1(BCF)}$ provide support for the ability of a Lewis acid to activate a Pd^0/1,3-enyne complex in an outer-sphere oxidative addition fashion. As a result, we conclude that among the mechanistic scenarios listed in Scheme 3, scenario (5) is the only mechanism that is fully consistent with the experimental observations presented thus far.

Next, we performed reaction progress kinetic analysis[27] to probe the kinetic features of the working reaction mechanism with the specific aim to gain insight into the possible resting state and the rate-limiting step of the catalytic cycle. We chose to employ $(cod)Pd(CH_2TMS)_2$[28] as the Pd precursor (vs Pd_2dba_3) to avoid potential complications with the dba serving as a competing ligand.[29] First, a same-excess experiment was conducted with enyne **1** as the limiting reagent. Plotting [**1**] vs time and applying a time adjustment, the adjusted trace (red triangle) and the initial trace (black dot) show overlay (Figure 1a), indicating that there is no catalyst deactivation or product inhibition during the reaction.[30] Then, different-"excess" experiments were conducted and analyzed using the Burés variable time normalization method[31] to determine the reaction orders of the reactants and the catalyst. As can be seen from the overlay plots, the reaction is zero order in enyne **1** (Figure 1b), first order in catecholborane **2** (Figure 1c), and first order in the Pd/Senphos catalyst (Figure 1d), resulting in the following rate expression:

$$\text{rate} = k_H[\mathbf{1}]^0[\mathbf{2}]^1[\text{Pd/Senphos}]^1 \quad (2)$$

With the experimental reaction orders established, the rate constant k_H in eq 2 can then be determined as $k_H = 0.90 \pm 0.042\ M^{-1}\cdot min^{-1}$ (see the Supporting Information). The corresponding rate constant for the reaction with a deuterated borane **2-D** is $k_D = 0.79 \pm 0.016\ M^{-1}\cdot min^{-1}$, resulting in a kinetic isotope effect (KIE = k_H/k_D) value of 1.1. It is worth noting that the primary KIE values involving breaking of B−H bonds are typically small in magnitude (<2.0).[32]

The obtained kinetic information is consistent with the proposed outer-sphere oxidative addition mechanism (Scheme 3, scenario (5)) where the resting state is the outer-sphere oxidative addition intermediate $\mathbf{Int_1}$ and the rate-limiting step being either the hydride abstraction or the hydride transfer step. The zero-order dependence in enyne **1** is the result of saturation kinetics due to the catalyst resting state, and the first-order dependence in borane **2** is due to the requirement of an additional borane as a hydride shuttle starting from the catalyst resting state.

The rate expression also explains the dependence of the *trans/cis* diastereoselectivity of the hydroboration on the borane concentration. As described in the double-crossover experiment section, a higher borane concentration favors the *trans*-hydroboration vs *cis*-hydroboration (see Figures S1 and S2). It is important to note that the resting state of the catalyst remains the outer-sphere oxidative addition intermediate $\mathbf{Int_1}$ for both the formation of the *trans*- and *cis*-hydroboration products. We already established that the *trans*-hydroboration reaction is first order in borane (eq 2). On the other hand, the *cis*-hydroboration reaction is expected to be zero order in borane; the transition state[20] (see Scheme 5) involves only one borane molecule, resulting in an "apparent saturation kinetics" with respect to the borane due to the catalyst resting state structure.[33] Thus, the first-order borane dependence for *trans* hydroboration vs predicted zero-order borane dependence for *cis* hydroboration is consistent with higher borane concentrations favoring the formation of the *trans* product.

Although our experimental data support in general the outer-sphere oxidative mechanism outlined by Shi *et al.* (Scheme 3, scenario (5)),[20] we do note several discrepancies between our experimental observations and Shi *et al.*'s computed reaction pathway. First, Shi *et al.*'s calculations predict product inhibition, but product inhibition is not observed in our reaction progress kinetic analysis. Second, Shi *et al.*'s calculations predict the Pd^0-bound product to be the resting state of the catalytic cycle, which is inconsistent with our kinetic analysis that rather assigns the outer-sphere oxidative addition adduct as the resting state. Shi *et al.*'s computed energy profile for the *trans*-hydroboration would predict a rate law that is first order in enyne and second order in borane (due to the resting state being the Pd^0-bound

https://doi.org/10.1021/acs.joc.2c02841
J. Org. Chem. 2023, 88, 2415−2424

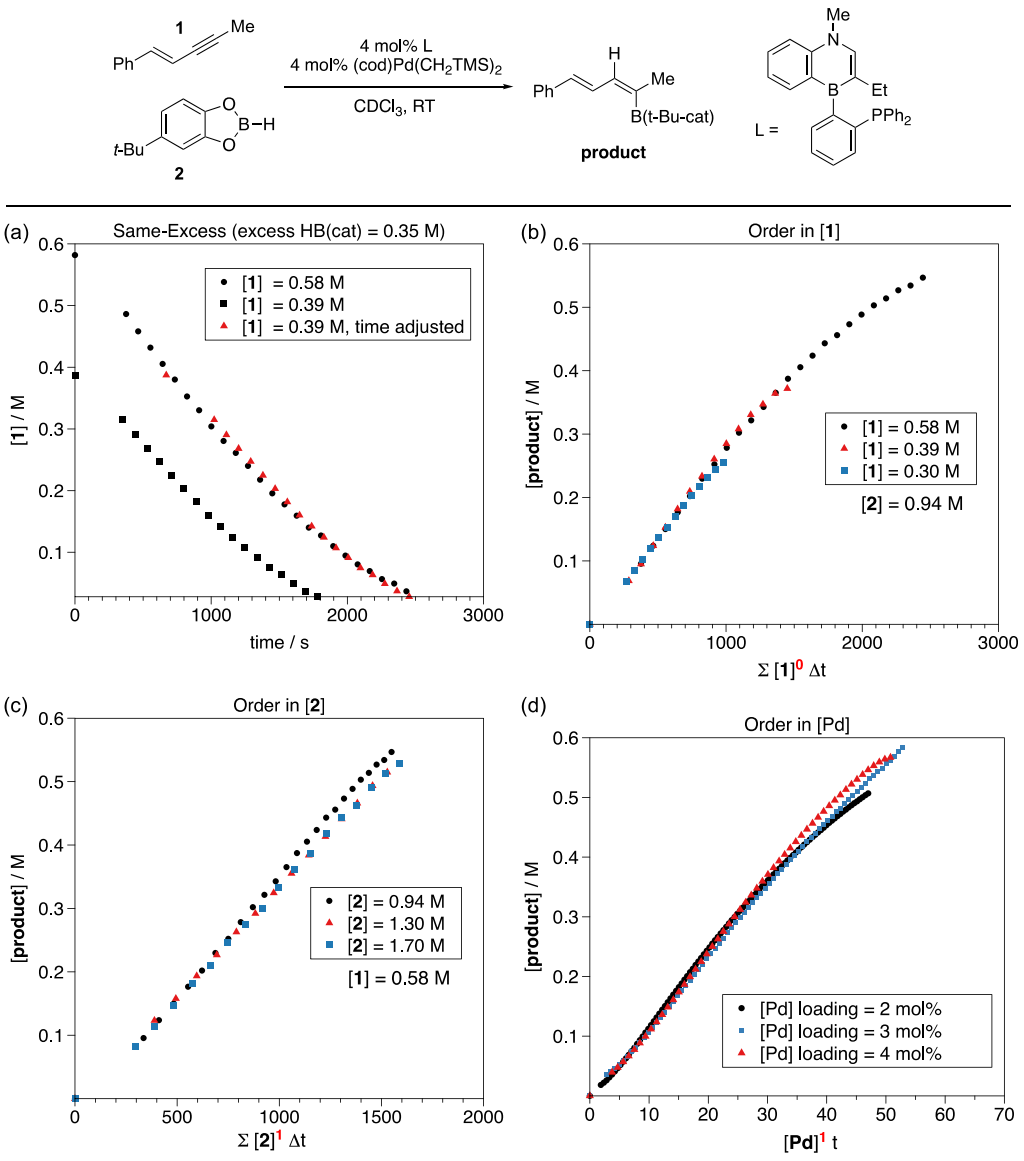

Figure 1. Reaction progress kinetic analysis: (a) same-excess experiment, (b) different-excess experiment to determine the reaction order in [**1**], (c) different-excess experiment to determine the reaction order in [**2**], and (d) varying [**Pd**] to determine the reaction order in [**Pd**] *via* variable time normalization.

product), which is not experimentally observed. Additionally, no transition state corresponding to a hydride transfer between boron and Pd has been located on the potential energy surface. In view of these discrepancies/shortcomings, we optimized the computational methods, accurately scrutinizing the potential energy surface (PES), and present here a refined reaction coordinate energy diagram for the Pd/Senphos catalyzed *trans*-hydroboration of 1,3-enyne **1**.

Density functional theory (DFT)[34] calculations were carried out at the SMD(CH_2Cl_2)[35,36]-TPSS[37]-D3(BJ)[38]/SDD+f-(Pd),[39] 6-31G**(other atoms) level of theory. The geometrical parameters of intermediates and transition states are available in the Supporting Information. Consistent with experimental data and previous calculations, this reaction occurs *via* an outer-sphere oxidative addition mechanism, where the Lewis acidic catecholborane (H-B(cat), blue color) activates the ***π*-complex** (i.e., enyne substrate bound to the Pd^0; the alkene-bound Pd^0 complex is determined to be more stable than the alkyne bound Pd complex by 7.0 kcal/mol), affording the outer-sphere oxidative addition adduct **Int_1** (Figure 2). In the next step, the borohydride is then transferred to a second H-B(cat) (red color). In contrast to Shi *et al.*'s calculations[20] where no transition state was attributed to this hydride transfer, we successfully located the associated transition states. Our calculations reveal that the hydride transfer process occurs in two steps, step 1: B−H bond activation (blue) by the shuttle borane (red) *via* **TS_2** (H(blue)···B(blue): 1.263 Å and H(blue)···B(red): 1.694 Å) to form hydride bridged diborane complex **Int_2** (H(blue)···B(blue): 1.344 Å, H(blue)···B(red): 1.387 Å, and ∠B(blue)−H(blue)−B(red): 180°) and step 2: hydride abstraction by the shuttle borane (red) *via* the rate-limiting **TS_3** to form **Int_3** where the $H_2B(cat)^-$ anion is completely released from the cationic Pd complex. Then, the $H_2B(cat)^-$ anion shifts toward the Pd^{II} metal in a barrierless process to form a precomplex **Int_4** with a hydride bridging the Pd and borane (Pd···H: 1.631 Å and B···H: 1.580 Å). In **Int_4**, we also note a change from a Pd-η^3-π-allyl coordination to a Pd-η^1-alkenyl coordination to

https://doi.org/10.1021/acs.joc.2c02841
J. Org. Chem. 2023, 88, 2415−2424

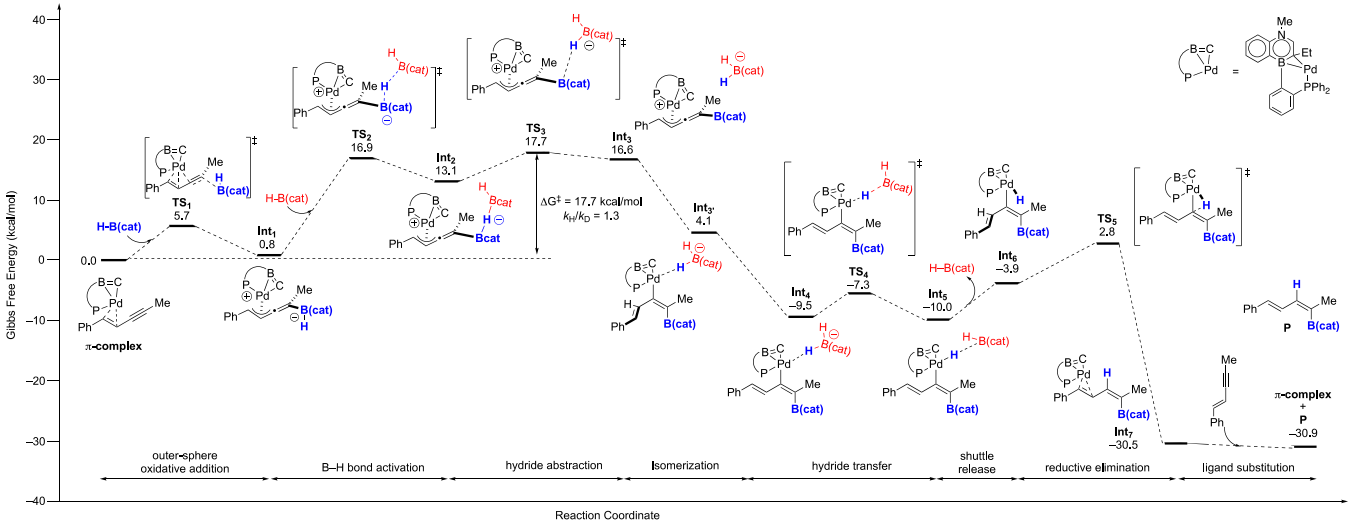

Figure 2. Energy profile (ΔG in kcal/mol) for the Pd/Senphos catalyzed *trans*-hydroboration process computed at the SMD(CH_2Cl_2)-TPSS-D3(BJ)BJ/SDD+f(Pd), 6-31G**(other atoms) level of theory.

maintain a 16e Pd^{II} configuration. A hydride is then transferred to Pd *via* transition state $\mathbf{TS_4}$, affording the η^1-alkenyl-Pd-hydride intermediate $\mathbf{Int_5}$ that might be very weakly coordinated to the leaving H-B(cat). In $\mathbf{TS_4}$, the Pd···H bond distance is 1.608 Å and the B···H distance is 1.711 Å, with a sum of bond angles around the boron atom $\Sigma_{\angle B}$: 354.2°. In $\mathbf{Int_5}$, the Pd···H bond distance is 1.583 Å and the B···H distance is 1.984 Å, with $\Sigma_{\angle B}$: 358.3°. It is worth noting that in Shi *et al.*'s calculations, the hydride transfer from boron to Pd was predicted to be the rate-limiting step. However, the corresponding transition state was located with a Pd···H bond distance of 5.087 Å, which is inconsistent with a hydride transfer. Rather, the located transition state more likely corresponds to the breaking of the Pd cation−arene (catecholborate) interaction. From $\mathbf{Int_5}$, the shuttle borane is released in a barrierless manner to form $\mathbf{Int_6}$, which then undergoes a three-centered reductive elimination *via* $\mathbf{TS_5}$ to furnish the product that is η^2-coordinated to the Pd catalyst ($\mathbf{Int_7}$). Ligand substitution with a new 1,3-enyne substrate starts a new catalytic cycle.

The present calculation formally identifies the Pd-enyne ***π*-complex** as the resting state of the catalyst with the caveat that the outer-sphere oxidative addition adduct $\mathbf{Int_1}$ can, within reasonable computational error range, be considered as the resting state as well.[40,41] With a predicted energy difference of less than 1.0 kcal/mol between the ***π*-complex** and $\mathbf{Int_1}$, it is possible that the equilibrium, and as a consequence the resting state, may be influenced by reaction stoichiometry (e.g., concentration of H-B(cat)) under the reaction conditions. The rate-limiting transition state $\mathbf{TS_3}$ involves the hydride abstraction step by the borane shuttle and is 17.7 kcal/mol above the resting state. This relatively small rate-limiting barrier ($\Delta G^{\ddagger}$) is consistent with the fast reaction times (15 min to 3.5 h) observed at room temperature. Finally, we calculated a KIE (k_H/k_D = 1.3) based on the illustrated reaction profile in Figure 2, which is in line with the observed experimental data (k_H/k_D = 1.1).

CONCLUSIONS

In summary, we investigated the reaction mechanism of the Pd/Senphos-catalyzed *trans*-hydroboration reaction of 1,3-enynes using various experimental techniques, including reaction progress kinetic analysis, X-ray crystallographic characterization of a model outer-sphere oxidative addition species, and double crossover labeling experiment.[42] Our experimental data establish catecholborane as a suitable electrophile to cooperatively activate the Pd^0-bound 1,3-enyne substrate *via* the unusual outer-sphere oxidative addition mechanism. The resulting outer-sphere oxidative addition adduct is proposed to be the resting state of the catalytic cycle and features the versatile Pd-η^3-π-allyl motif and the characteristic κ^2-η^2-BC-coordination by the Senphos ligand as evidenced by single-crystal structure analysis of the model compound. The results of the double crossover labeling of the catecholborane are consistent with the borane serving an additional role as a hydride shuttle. We also refined a previously reported computational mechanistic study and determined that the rate-limiting transition state of the reaction is the hydride abstraction by the catecholborane shuttle, which is consistent with the experimentally determined rate law. The computed activation free energy $\Delta G^{\ddagger}$ = 17.7 kcal/mol and KIE (k_H/k_D = 1.3) are also in line with experimental observations. Overall, this work experimentally establishes Lewis acids such as catecholborane as viable electrophilic activators to engage in an outer-sphere oxidative addition reaction and points toward outer-sphere oxidative addition as a likely general approach to activate unsaturated substrates.

ASSOCIATED CONTENT

Data Availability Statement

The data underlying this study are available in the published article and its Supporting Information.

Supporting Information

The Supporting Information is available free of charge at https://pubs.acs.org/doi/10.1021/acs.joc.2c02841.

Experimental procedures, compound characterization data, and computational and crystallographic information (PDF)

Optimized Cartesian coordinates (XYZ)

https://doi.org/10.1021/acs.joc.2c02841
J. Org. Chem. 2023, 88, 2415−2424

Accession Codes

CCDC 2211462 contains the supplementary crystallographic data for this paper. These data can be obtained free of charge via www.ccdc.cam.ac.uk/data_request/cif, or by emailing data_request@ccdc.cam.ac.uk, or by contacting The Cambridge Crystallographic Data Centre, 12 Union Road, Cambridge CB2 1EZ, UK; fax: +44 1223 336033.

AUTHOR INFORMATION

Corresponding Authors

Karinne Miqueu − *E2S UPPA/CNRS, Université de Pau et des Pays de l'Adour, Institut des Sciences Analytiques et de Physico-Chimie pour l'Environnement et les Matériaux IPREM UMR 5254. Hélioparc, 64053 Pau, France;* orcid.org/0000-0002-5960-1877; Email: karinne.miqueu@univ-pau.fr

Shih-Yuan Liu − *Department of Chemistry, Boston College, Chestnut Hill, Massachusetts 02467-3860, United States; E2S UPPA/CNRS, Université de Pau et des Pays de l'Adour, Institut des Sciences Analytiques et de Physico-Chimie pour l'Environnement et les Matériaux IPREM UMR 5254. Hélioparc, 64053 Pau, France;* orcid.org/0000-0003-3148-9147; Email: shihyuan.liu@bc.edu

Authors

Yuanzhe Zhang − *Department of Chemistry, Boston College, Chestnut Hill, Massachusetts 02467-3860, United States*

Ziyong Wang − *Department of Chemistry, Boston College, Chestnut Hill, Massachusetts 02467-3860, United States*

Walid Lamine − *E2S UPPA/CNRS, Université de Pau et des Pays de l'Adour, Institut des Sciences Analytiques et de Physico-Chimie pour l'Environnement et les Matériaux IPREM UMR 5254. Hélioparc, 64053 Pau, France*

Senmiao Xu − *Department of Chemistry, Boston College, Chestnut Hill, Massachusetts 02467-3860, United States;* Present Address: State Key Laboratory for Oxo Synthesis and Selective Oxidation, Center for Excellence in Molecular Synthesis, Suzhou Research Institute, Lanzhou Institute of Chemical Physics, Chinese Academy of Sciences, Lanzhou 730000, People's Republic of China (S.X.); orcid.org/0000-0003-0249-8765

Bo Li − *Department of Chemistry, Boston College, Chestnut Hill, Massachusetts 02467-3860, United States*

Anna Chrostowska − *E2S UPPA/CNRS, Université de Pau et des Pays de l'Adour, Institut des Sciences Analytiques et de Physico-Chimie pour l'Environnement et les Matériaux IPREM UMR 5254. Hélioparc, 64053 Pau, France*

Complete contact information is available at: https://pubs.acs.org/10.1021/acs.joc.2c02841

Notes

The authors declare no competing financial interest.

ACKNOWLEDGMENTS

Research reported in this publication was supported by the National Institute of General Medical Sciences of the National Institutes of Health (NIGMS) under award number R01GM136920, the Excellence Initiative of Université de Pau et des Pays de l'Adour I-Site E2S UPPA, and by Boston College start-up funds. We also acknowledge the NIH-S10 (award 1S10OD026910-01A1) and the NSF-MRI (award CHE-2117246) for the support of Boston College's NMR facilities. The "Direction du Numérique" of the Université de Pau et des Pays de l'Adour (UPPA), CINES under allocation A011080045 made by Grand Equipement National de Calcul Intensif (GENCI), and Mésocentre de Calcul Intensif Aquitain (MCIA) are acknowledged for the support of computational facilities. Y.Z. and Z.W. were supported as LaMattina Graduate Fellows in Chemical Synthesis. We thank Dr. Jean-Marc Sotiropoulos and Dr. Thusitha Jayasundera for helpful discussions.

REFERENCES

(1) For a recent overview, see Pàmies, O.; Margalef, J.; Cañellas, S.; James, J.; Judge, E.; Guiry, P. J.; Moberg, C.; Backvall, J. E.; Pfaltz, A.; Pericàs, M. A.; Dieguez, M. Recent Advances in Enantioselective Pd-Catalyzed Allylic Substitution: From Design to Applications. *Chem. Rev.* **2021**, *121*, 4373−4505.

(2) For a recent overview, see (a) Trost, B. M.; Crawley, M. L. Asymmetric transition-metal-catalyzed allylic alkylations: applications in total synthesis. *Chem. Rev.* **2003**, *103*, 2921−2944. For examples of (1,2,3-η^3-butadien-3-yl)-palladium complexes, see (b) Ogasawara, M.; Okada, A.; Watanabe, S.; Fan, L.; Uetake, K.; Nakajima, K.; Takahashi, T. Synthesis, structure, and reactivity of (1,2,3-eta(3)-butadien-3-yl)-palladium complexes. *Organometallics* **2007**, *26*, 5025−5029.

(3) For a recent overview, see (a) Wang, P. S.; Gong, L. Z. Palladium-Catalyzed Asymmetric Allylic C-H Functionalization: Mechanism, Stereo- and Regioselectivities, and Synthetic Applications. *Acc. Chem. Res.* **2020**, *53*, 2841−2854. (b) Fernandes, R. A.; Nallasivam, J. L. Catalytic allylic functionalization via pi-allyl palladium chemistry. *Org. Biomol. Chem.* **2019**, *17*, 8647−8672.

(4) For an overview, see (a) Zimmer, R.; Dinesh, C. U.; Nandanan, E.; Khan, F. A. Palladium-catalyzed reactions of allenes. *Chem. Rev.* **2000**, *100*, 3067−3126. (b) Bates, R. W.; Satcharoen, V. Nucleophilic transition metal-based cyclization of allenes. *Chem. Soc. Rev.* **2002**, *31*, 12−21.

(5) For an overview, see (a) Wu, X.; Gong, L. Z. Palladium(0)-Catalyzed Difunctionalization of 1,3-Dienes: From Racemic to Enantioselective. *Synthesis* **2019**, *51*, 122−134. For select examples, see (b) Park, S.; Malcolmson, S. J. Development and Mechanistic Investigations of Enantioselective Pd-Catalyzed Intermolecular Hydroaminations of Internal Dienes. *ACS Catal.* **2018**, *8*, 8468−8476. (c) Adamson, N. J.; Jeddi, H.; Malcolmson, S. J. Preparation of Chiral Allenes through Pd-Catalyzed Intermolecular Hydroamination of Conjugated Enynes: Enantioselective Synthesis Enabled by Catalyst Design. *J. Am. Chem. Soc.* **2019**, *141*, 8574−8583.

(6) For select examples, see: (a) Bar, G. L. J.; Lloyd-Jones, G. C.; Booker-Milburn, K. I. Pd(II)- Catalyzed Intermolecular 1,2-Diamination of Conjugated Dienes. *J. Am. Chem. Soc.* **2005**, *127*, 7308−7309. (b) Coscia, R. W.; Lambert, T. H. Development of a Formal [4 + 1] Cycloaddition: $Pd(OAc)_2$-Catalyzed Intramolecular Cyclopropanation of 1,3-Dienyl β-Keto Esters and MgI_2-Promoted Vinylcyclopropane- Cyclopentene Rearrangement. *J. Am. Chem. Soc.* **2009**, *131*, 2496−2498. (c) Wu, M.-S.; Fan, T.; Chen, S.-S.; Han, Z.-Y.; Gong, L.-Z. Pd(II)- Catalyzed Asymmetric Oxidative 1,2-Diamination of Conjugated Dienes with Ureas. *Org. Lett.* **2018**, *20*, 2485−2489.

(7) Camacho, D. H.; Saito, S.; Yamamoto, Y. 'Anti-Wacker'-type hydroalkoxylation of diynes catalyzed by palladium(0). *Tetrahedron Lett.* **2002**, *43*, 1085−1088.

(8) Stoichiometric activation of unsaturated substrates by low-valent metals with an electrophile has been reported. For examples, see (a) Liebov, B. K.; Harman, W. D. Group 6 Dihapto-Coordinate Dearomatization Agents for Organic Synthesis. *Chem. Rev.* **2017**, *117*, 13721−13755. (b) Casey, C. P.; Chung, S.; Ha, Y.; Powell, D. R. Formation of platinum allyl and propargyl complexes from protonation of platinum enyne and diyne complexes. *Inorg. Chim. Acta* **1997**, *265*, 127−138. (c) Casey, C. P.; Chung, S. Protonation of rhenium 1,3-enyne and 1,3-diyne complexes: formation of exo-

alkylidene eta-3-allyl and eta-3-propargyl complexes. *Inorg. Chim. Acta* **2002**, *334*, 283−293.
(9) The authors used the term "*anti*-selective hydropalladation" to describe the critical oxidative addition step, see Tsukamoto, H.; Konno, T.; Ito, K.; Doi, T. Palladium(0)-Lithium Iodide Co-catalyzed Asymmetric Hydroalkylation of Conjugated Enynes with Pronucleophiles Leading to 1,3-Disubstituted Allenes. *Org. Lett.* **2019**, *21*, 6811−6814.
(10) (a) Xiao, B. X.; Jiang, B.; Yan, R. J.; Zhu, J. X.; Xie, K.; Gao, X. Y.; Ouyang, Q.; Du, W.; Chen, Y. C. A Palladium Complex as an Asymmetric π-Lewis Base Catalyst for Activating 1,3-Dienes. *J. Am. Chem. Soc.* **2021**, *143*, 4809−4816. (b) He, Q.; Zhu, L.; Yang, Z. H.; Zhu, B.; Ouyang, Q.; Du, W.; Chen, Y. C. Palladium-Catalyzed Modular and Enantioselective *cis*-Difunctionalization of 1,3-Enynes with Imines and Boronic Reagents. *J. Am. Chem. Soc.* **2021**, *143*, 17989−17994.
(11) Xu, S.; Zhang, Y.; Li, B.; Liu, S.-Y. Site-Selective and Stereoselective *trans*-Hydroboration of 1,3-Enynes Catalyzed by 1,4-Azaborine-Based Phosphine-Pd Complex. *J. Am. Chem. Soc.* **2016**, *138*, 14566−14569.
(12) (a) Xu, S.; Haeffner, F.; Li, B.; Zakharov, L. N.; Liu, S.-Y. Monobenzofused 1,4-azaborines: synthesis, characterization, and discovery of a unique coordination mode. *Angew. Chem., Int. Ed.* **2014**, *53*, 6795−6799. (b) Zhang, Y.; Li, B.; Liu, S.-Y. Pd-Senphos Catalyzed *trans*-Selective Cyanoboration of 1,3-Enynes. *Angew. Chem., Int. Ed.* **2020**, *59*, 15928−15932. (c) Wang, Z.; Wu, J.; Lamine, W.; Li, B.; Sotiropoulos, J. M.; Chrostowska, A.; Miqueu, K.; Liu, S.-Y. C-Boron Enolates Enable Palladium Catalyzed Carboboration of Internal 1,3-Enynes. *Angew. Chem., Int. Ed.* **2021**, *60*, 21231−21236.
(13) For an example of an amine-directed, AuI-catalyzed *trans*-hydroboration of propargylic amines, see Wang, Q.; Motika, S. E.; Akhmedov, N. G.; Petersen, J. L.; Shi, X. Synthesis of Cyclic Amine Boranes through Triazole-Gold(I)-Catalyzed Alkyne Hydroboration. *Angew. Chem., Int. Ed.* **2014**, *53*, 5418−5422.
(14) For select transition metal-free *trans*-hydroboration reactions, see (a) Yuan, K.; Suzuki, N.; Mellerup, S. K.; Wang, X.; Yamaguchi, S.; Wang, S. Pyridyl Directed Catalyst-Free *trans*-Hydroboration of Internal Alkynes. *Org. Lett.* **2016**, *18*, 720−723. (b) McGough, J. S.; Butler, S. M.; Cade, I. A.; Ingleson, M. J. Highly selective catalytic *trans*-hydroboration of alkynes mediated by borenium cations and $B(C_6F_5)_3$. *Chem. Sci.* **2016**, *7*, 3384−3389. (c) Fritzemeier, R.; Gates, A.; Guo, X.; Lin, Z.; Santos, W. L. Transition Metal-Free *Trans* Hydroboration of Alkynoic Acid Derivatives: Experimental and Theoretical Studies. *J. Org. Chem.* **2018**, *83*, 10436−10444. (d) Grams, R. J.; Fritzemeier, R. G.; Slebodnick, C.; Santos, W. L. *trans*-Hydroboration of Propiolamides: Access to Primary and Secondary (E)-β-Borylacrylamides. *Org. Lett.* **2019**, *21*, 6795−6799. (e) Bowen, J.; Slebodnick, C.; Santos, W. L. Phosphine-catalyzed hydroboration of propiolonitriles: access to (E)-1,2-vinylcyanotrifluoroborate derivatives. *Chem. Commun.* **2022**, *58*, 5984−5987. (f) Jos, S.; Szwetkowski, C.; Slebodnick, C.; Ricker, R.; Chan, K. L.; Chan, W. C.; Radius, U.; Lin, Z.; Marder, T. B.; Santos, W. L. Transition Metal-Free Regio- and Stereo-Selective *trans* Hydroboration of 1,3-Diynes: A Phosphine-Catalyzed Access to (E)-1-Boryl-1,3-Enynes. *Chem. − Eur. J.* **2022**, No. e202202349.
(15) Ohmura, T.; Yamamoto, Y.; Miyaura, N. Rhodium- or Iridium-Catalyzed *trans*-Hydroboration of Terminal Alkynes, Giving (Z)-1-Alkenylboron Compounds. *J. Am. Chem. Soc.* **2000**, *122*, 4990−4991.
(16) Gunanathan, C.; Hölscher, M.; Pan, F.; Leitner, W. Ruthenium catalyzed hydroboration of terminal alkynes to Z-vinylboronates. *J. Am. Chem. Soc.* **2012**, *134*, 14349−14352.
(17) Obligacion, J. V.; Neely, J. M.; Yazdani, A. N.; Pappas, I.; Chirik, P. J. Cobalt catalyzed Z-selective hydroboration of terminal alkynes and elucidation of the origin of selectivity. *J. Am. Chem. Soc.* **2015**, *137*, 5855−5858.
(18) Sundararaju, B.; Fürstner, A. A *trans*-selective hydroboration of internal alkynes. *Angew. Chem., Int. Ed.* **2013**, *52*, 14050−14054.
(19) For a mechanistic analysis of the analogous hydrosilylation of alkynes catalyzed by cationic ruthenium complexes, see Chung, L. W.; Wu, Y. D.; Trost, B. M.; Ball, Z. T. A theoretical study on the mechanism, regiochemistry, and stereochemistry of hydrosilylation catalyzed by cationic ruthenium complexes. *J. Am. Chem. Soc.* **2003**, *125*, 11578−11582.
(20) Yang, Y.; Jiang, J.; Yu, H.; Shi, J. Mechanism and Origin of the Stereoselectivity in the Palladium-Catalyzed *trans* Hydroboration of Internal 1,3-Enynes with an Azaborine-Based Phosphine Ligand. *Chem. − Eur. J.* **2018**, *24*, 178−186.
(21) (a) Narayana, C.; Periasamy, M. A simple convenient method for the generation of diborane from $NaBH_4$ and I_2. *J. Organomet. Chem.* **1987**, *323*, 145−147. (b) Suseela, Y.; Prasad, A. S. B.; Periasamy, M. Catalytic effect of a BH_3: *N,N*-diethylaniline complex in the formation of alkenyl catecholboranes from alk-1-ynes and catecholborane. *Chem. Commun.* **1990**, *6*, 446−447. (c) Safronov, A. V.; Jalisatgi, S. S.; Hawthorne, M. F. Novel Convenient Synthesis of -^{10}B-Enriched Sodium Borohydride. *Inorg. Chem.* **2016**, *55*, 5116−5117.
(22) Isotopically labeled 4-*t*-Bu-catecholborane is more easily purified. For direct comparative purposes (labeled vs unlabeled), 4-*t*-Bu-catecholborane was chosen as the borane reagent.
(23) The ratios reported in Scheme 5 represent the directly observed relative intensities of **3-trans** and **3-cis** with the corresponding molecular weights (269, 270, and 271) from the MS instrument. Corrections for natural abundance (e.g., the presence of 1% ^{13}C) have not been made. We estimate that accounting for these corrections would lead to an error of ±10%, which would make this method unsuitable for evaluating small kinetic isotope effects.
(24) Brown, J. M.; Lloyd-Jones, G. C. Vinylborane Formation in Rhodium-Catalyzed Hydroboration of Vinylarenes. Mechanism versus Borane Structure and Relationship to Silation. *J. Am. Chem. Soc.* **1994**, *116*, 866−878.
(25) For example, conditions shown in Scheme 5, entry 1 ($[borane]_{total}$ = 0.14 M and [borane]/[enyne] = 0.11) lead to low *trans:cis* selectivity (~1:1 in the first 2 min period). However, as the borane concentration doubled (Scheme 5, entry 2, $[borane]_{total}$ = 0.28 M and [borane]/[enyne] = 0.22), the *trans:cis* selectivity increases to 7:1. In a standard *trans*-hydroboration reaction, the borane concentration is >1.25 M ([borane]/[enyne] = 1.5).
(26) For an overview of $B(C_6F_5)_3$-mediated activation of small molecules, see (a) Stephan, D. W. Catalysis, FLPs, and Beyond. *Chem* **2020**, *6*, 1520−1526. (b) Lam, J.; Szkop, K. M.; Mosaferi, E.; Stephan, D. W. FLP catalysis: main group hydrogenations of organic unsaturated substrates. *Chem. Soc. Rev.* **2019**, *48*, 3592−3612.
(27) Blackmond, D. G. Reaction progress kinetic analysis: a powerful methodology for mechanistic studies of complex catalytic reactions. *Angew. Chem., Int. Ed.* **2005**, *44*, 4302−4320.
(28) (a) Pan, Y. Y. B. Syntheses and spectroscopic characteristics of dialkylpalladium(II) complexes; PdR_2(cod) as precursors for derivatives with N- or P-donor ligands. *J. Organomet. Chem.* **1999**, *577*, 257−264. (b) Sergeev, A. G.; Schulz, T.; Torborg, C.; Spannenberg, A.; Neumann, H.; Beller, M. Palladium-catalyzed hydroxylation of aryl halides under ambient conditions. *Angew. Chem., Int. Ed.* **2009**, *48*, 7595−7599. (c) Lee, H. G.; Milner, P. J.; Buchwald, S. L. An improved catalyst system for the Pd-catalyzed fluorination of (hetero)aryl triflates. *Org. Lett.* **2013**, *15*, 5602−5605. (d) Takahashi, R.; Kubota, K.; Ito, H. Air- and moisture-stable Xantphos-ligated palladium dialkyl complex as a precatalyst for cross-coupling reactions. *Chem. Commun.* **2020**, *56*, 407−410.
(29) (a) Fairlamb, I. J.; Kapdi, A. R.; Lee, A. F.; McGlacken, G. P.; Weissburger, F.; de Vries, A. H.; Schmieder Van de Vondervoort, L. Exploiting noninnocent (*E,E*)-dibenzylideneacetone (dba) effects in palladium(0)-mediated cross-coupling reactions: modulation of the electronic properties of dba affects catalyst activity and stability in ligand and ligand-free reaction systems. *Chem. − Eur. J.* **2006**, *12*, 8750−8761. (b) Fairlamb, I. J. pi-Acidic alkene ligand effects in Pd-catalysed cross-coupling processes: exploiting the interaction of dibenzylidene acetone (dba) and related ligands with Pd(0) and Pd(II). *Org. Biomol. Chem.* **2008**, *6*, 3645−3656. (c) Colletto, C.; Burés, J.; Larrosa, I. Reaction monitoring reveals poisoning

https://doi.org/10.1021/acs.joc.2c02841
J. Org. Chem. 2023, 88, 2415−2424

mechanism of $Pd_2(dba)_3$ and guides catalyst selection. *Chem. Commun.* **2017**, *53*, 12890−12893.
(30) (a) Baxter, R. D.; Sale, D.; Engle, K. M.; Yu, J. Q.; Blackmond, D. G. Mechanistic rationalization of unusual kinetics in Pd-catalyzed C-H olefination. *J. Am. Chem. Soc.* **2012**, *134*, 4600−4606. (b) Blackmond, D. G. Kinetic Profiling of Catalytic Organic Reactions as a Mechanistic Tool. *J. Am. Chem. Soc.* **2015**, *137*, 10852−10866.
(31) (a) Bures, J. A Simple Graphical Method to Determine the Order in Catalyst. *Angew. Chem., Int. Ed.* **2016**, *55*, 2028−2031. (b) Bures, J. Variable Time Normalization Analysis: General Graphical Elucidation of Reaction Orders from Concentration Profiles. *Angew. Chem., Int. Ed.* **2016**, *55*, 16084−16087.
(32) (a) Hawthorne, M. F.; Lewis, E. S.; Boranes, A., III Hydrolysis of Pyridine Diphenylborane and the Mechanism of Hydride Transfer Reactions. *J. Am. Chem. Soc.* **1958**, *80*, 4296−4299. (b) Wigfield, D. C.; Phelps, D. J. Deuterium Isotope Effects in the Reduction of Cyclohexanones The Concepts of Steric Approach Control and Product Development Control. *Can. J. Chem.* **1972**, *50*, 388−394. (c) Leitao, E. M.; Stubbs, N. E.; Robertson, A. P.; Helten, H.; Cox, R. J.; Lloyd-Jones, G. C.; Manners, I. Mechanism of metal-free hydrogen transfer between amine-boranes and aminoboranes. *J. Am. Chem. Soc.* **2012**, *134*, 16805−16816.
(33) The TS for **3-cis** (where the Pd and B(cat) are on the same face of the resulting alkene) is achieved from the proposed catalyst resting state $\mathbf{Int_1}$ (Pd and B(cat) are on the opposite face of the alkene) *via* the starting Pd(0)-enyne complex by first dissociating H-B(cat) from $\mathbf{Int_1}$. With a calculated free energy barrier of <6.0 kcal/mol, the outer-sphere oxidative addition step is readily reversible under the reaction conditions. The Pd(0)-enyne complex then engages with H-B(cat) *via* the TS for **3-cis**. As the catalyst resting state for the formation of **3-cis** should also be $\mathbf{Int_1}$, kinetically speaking (using the quasi-equilibrium approach), the formation of **3-cis** (with the TS for **3-cis** being the rate-limiting TS) should be zero order with respect to [H-B(cat)], consistent with our experimental observations.
(34) Frisch, M. J.; Trucks, G. W.; Schlegel, H. B.; Scuseria, G. E.; Robb, M. A.; Cheeseman, J. R.; Scalmani, G.; Barone, V.; Mennucci, B.; Petersson, G. A.; Nakatsuji, H.; Caricato, M.; Li, X.; Hratchian, H. P.; Izmaylov, A. F.; Bloino, J.; Zheng, G.; Sonnenberg, J. L.; Hada, M.; Ehara, M.; Toyota, K.; Fukuda, R.; Hasegawa, J.; Ishida, M.; Nakajima, T.; Honda, Y.; Kitao, O.; Nakai, H.; Vreven, T.; Montgomery, J. A., Jr.; Peralta, J. E.; Ogliaro, F.; Bearpark, M.; Heyd, J. J.; Brothers, E.; Kudin, K. N.; Staroverov, V. N.; Kobayashi, R.; Normand, J.; Raghavachari, K.; Rendell, A.; Burant, J. C.; Iyengar, S. S.; Tomasi, J.; Cossi, M.; Rega, N.; Millam, J. M.; Klene, M.; Knox, J. E.; Cross, J. B.; Bakken, V.; Adamo, C.; Jaramillo, J.; Gomperts, R.; Stratmann, R. E.; Yazyev, O.; Austin, A. J.; Cammi, R.; Pomelli, C.; Ochterski, J. W.; Martin, R. L.; Morokuma, K.; Zakrzewski, V. G.; Voth, G. A.; Salvador, P.; Dannenberg, J. J.; Dapprich, S.; Daniels, A. D.; Farkas, Ö.; Foresman, J. B.; Ortiz, J. V.; Cioslowski, J.; Fox, D. J. *Gaussian 09, Revision D.01*; Gaussian, Inc., Wallingford CT, 2009.
(35) The reported optimized conditions involve CH_2Cl_2 as the solvent, see the Supporting Information for computational details.
(36) Marenich, A. V.; Cramer, C. J.; Truhlar, D. G. Universal solvation model based on solute electron density and on a continuum model of the solvent defined by the bulk dielectric constant and atomic surface tensions. *J. Phys. Chem. B* **2009**, *113*, 6378−6396.
(37) Tao, J.; Perdew, J. P.; Staroverov, V. N.; Scuseria, G. E. Climbing the density functional ladder: nonempirical meta-generalized gradient approximation designed for molecules and solids. *Phys. Rev. Lett.* **2003**, *91*, No. 146401.
(38) (a) Grimme, S.; Antony, J.; Ehrlich, S.; Krieg, H. A consistent and accurate *ab initio* parametrization of density functional dispersion correction (DFT-D) for the 94 elements H-Pu. *J. Chem. Phys.* **2010**, *132*, 154104. (b) Grimme, S.; Ehrlich, S.; Goerigk, L. Effect of the damping function in dispersion corrected density functional theory. *J. Comput. Chem.* **2011**, *32*, 1456−1465.
(39) Ehlers, A. W.; Bohme, M.; Dapprich, S.; Gobbi, A.; Hollwarth, A.; Jonas, V.; Kohler, K. F.; Stegmann, R.; Veldkamp, A.; Frenking, G. A Set of F-Polarization Functions for Pseudo-Potential Basis-Sets of the Transition-Metals Sc-Cu Y-Ag and La-Au. *Chem. Phys. Lett.* **1993**, *208*, 111−114.
(40) The accuracy of DFT methods has been evaluated. For leading references, see (a) Hopmann, K. How Accurate is DFT for Iridium-Mediated Chemistry? *Organometallics* **2016**, *35*, 3795−3807. (b) Gusev, D. G. Assessing the Accuracy of M06-L Organometallic Thermochemistry. *Organometallics* **2013**, *32*, 4239−4243.
(41) An error range of a 1−2 kcal/mol in DFT calculations has been reported. For an example, see Chan, A. P. Y.; Jakoobi, M.; Wang, C.; O'Neill, R. T.; Aydin, G. S. S.; Halcovitch, N.; Boulatov, R.; Sergeev, A. G. Selective ortho-C-H Activation in Arenes without Functional Groups. *J. Am. Chem. Soc.* **2022**, *144*, 11564−11568.
(42) A version of this manuscript has been deposited on ChemRxiv: Zhang, Y.; Wang, Z.; Wu Lamine, W.; Xu, S.; Li, B.; Chrostowska, A.; Miqueu, K.; Liu, S.-Y., Mechanism of Pd/Senphos-Catalyzed trans-Hydroboration of 1,3-Enynes: Experimental and Computational Evidence in Support of the Unusual Outer-Sphere Oxidative Addition Pathway. *ChemRxiv* **2022**, October 6 , 2022. DOI: 10.26434/chemrxiv-2022-cmzdf.